A Fast, Time-Accurate, Unsteady Full Potential Scheme

Vijaya Shankar,* Hiroshi Ide,† Joseph Gorski‡
Rockwell International Science Center, Thousand Oaks, California

and

Stanley Osher§
University of California, Los Angeles

The unsteady form of the full potential equation is solved in conservation form by an implicit method based on approximate factorization. At each time level, internal Newton iterations are performed to achieve time accuracy and computational efficiency. A local time linearization procedure is introduced to provide a good initial guess for the Newton iteration. A flux biasing technique is applied to generate proper forms of the artificial viscosity to treat hyperbolic regions with shocks and sonic lines present. The wake is modeled by a cut behind the trailing edge across which the density is matched at any instant of time by solving the vorticity convection equation. The far field is modeled using the Riemann invariants to simulate nonreflecting boundary conditions. The resulting unsteady method performs well and, even at low reduced frequency levels of 0.1 or less, requires fewer than 100 time steps per cycle at transonic Mach numbers.

I. Introduction

NONLINEAR aerodynamic prediction methods based on the steady form of the full potential equation are used regularly for treating transonic[1,2] and supersonic[3-6] flows over realistic wing-body configurations. Numerical algorithms to compute the unsteady form of the full potential equation are still in a developmental stage, and several researchers[7-11] have recently made significant progress in this area. There are several issues involved in the construction of a robust and efficient numerical algorithm for the unsteady full potential equation. They are: 1) proper treatment of boundary conditions in a nonorthogonal grid system, 2) correct formulation for the production of artificial viscosity to capture shocks, 3) proper concepts for time linearization and for accurate treatment of time derivative terms, 4) unsteady wake treatment, and 5) nonreflecting outer boundary conditions.

The objective of the present paper is to present a numerical treatment of the unsteady full potential equation that properly takes into account the importance of the items listed above. The paper discusses a local time linearization procedure coupled with a Newton iteration technique, a flux biasing concept based on sonic conditions (instead of the usual density biasing procedures) for the treatment of spatial derivative terms, split boundary condition procedures consistent with approximate factorization schemes, unsteady wake models with proper jumps in ϕ and higher derivatives of ϕ taken into account from density relationships, and nonreflecting unsteady far-field procedures based on Riemann invariants derived from the characteristic theory.

Use of unsteady methods has application not only to unsteady problems, but also to time asymptotic steady-state solutions. Also, in the unsteady method, since the time direction is always present, the hyperbolicity of the unsteady full potential equation will allow one to obtain solutions to problems across the Mach number range (subsonic, transonic, and supersonic), whether steady or unsteady. However, for purely supersonic flows, the marching technique of Refs. 4-6 is the most efficient procedure to apply. A unified full potential scheme within the unsteady framework of this paper, which includes the marching technique of Refs. 4-6 for treatment of supersonic flows as a special case, is reported in Ref. 12.

Results are presented for flows over steady and unsteady pitching airfoils at various Mach numbers and at reduced frequencies, and comparisons are made with experimental data. Use of the split boundary condition technique, combined with the flux biasing concepts[13,14] and the internal Newton iteration, has resulted in a robust method which, even for a difficult case with a fishtail shock at the trailing edge, did not require any code adjustments. The method performs well even at low reduced frequencies of 0.1 or less, requiring fewer than 100 time steps per cycle.

II. Formulation

The two-dimensional, unsteady full potential equation written in a body-fitted coordinate system represented by $\tau = t$, $\zeta = \zeta(x, y, t)$, and $\eta = \eta(x, y, t)$ takes the form

$$\left(\frac{\rho}{J}\right)_\tau + \left(\rho\frac{U}{J}\right)_\zeta + \left(\rho\frac{V}{J}\right)_\eta = 0 \tag{1}$$

where

$$\rho = \text{density} = \left[1 - \frac{\gamma-1}{2}M_\infty^2\left(2\phi_\tau + \bar{U}\phi_\zeta + \bar{V}\phi_\eta - 1\right)\right]^{1/(\gamma-1)}$$

$$U = \zeta_t + a_{11}\phi_\zeta + a_{12}\phi_\eta;\ \bar{U} = U + \zeta_t$$

$$V = \eta_t + a_{12}\phi_\zeta + a_{22}\phi_\eta;\ \bar{V} = V + \eta_t$$

$$a_{11} = \zeta_x^2 + \zeta_y^2;\ a_{12} = \zeta_x\eta_x + \zeta_y\eta_y$$

$$a_{22} = \eta_x^2 + \eta_y^2$$

$$J = \text{Jacobian} = \zeta_x\eta_y - \zeta_y\eta_y$$

Presented as Paper 85-1512 at the AIAA Seventh Computational Fluid Dynamics Conference, July 15-17, 1985; received July 23, 1985; revision received June 11, 1986.

*Manager, Computational Fluid Dynamics Department. Associate Fellow AIAA.
†Member Technical Staff, Aircraft Operations.
‡Technical Specialist. Member AIAA.
§Professor, Department of Mathematics. Member AIAA.

The density ρ and the fluxes ρU and ρV are complicated nonlinear functions of ϕ, the velocity potential.

Let n be the running index in the time direction, k in the ζ direction, and j in the η direction leading out of the surface. The objective is to solve Eq. (1) for $\phi_{j,k}^{n+1}$ at the current time plane, knowing the information at $n, n-1, n-2, \cdots$ planes.

Let Eq. (1) be represented as

$$F(\phi) = 0 \tag{2}$$

where ϕ is the unknown to be solved for at every grid point (j, k) in the $(n+1)$ plane. The Newton iteration for solution to Eq. (2) is

$$F(\phi_*) + \left(\frac{\partial F}{\partial \phi}\right)_{\phi=\phi_*} (\phi - \phi_*) = 0 \tag{3}$$

where ϕ_* is the currently available value of ϕ at the $(n+1)$ level. At convergence, $\Delta\phi = \phi - \phi_*$ will approach zero. Execution of Eq. (3) requires an initial guess for ϕ at $(n+1)$ to initiate the Newton iteration process.

The solution procedure to Eq. (1) will have two steps:

1) Generation of an initial guess for ϕ at $(n+1)$ using a time linearization procedure. In general, the initial guess for ϕ set to be $\phi_{j,k}^{n}$ will work. However, for large Δt calculations or for rapidly varying unsteady phenomena, the choice of initial guess is crucial for convergence of the Newton iteration process. The time linearization procedure for generation of the initial guess, to be presented later in this paper, is an efficient and robust method.

2) Starting with the initial guess from step 1, perform the Newton iteration of Eq. (3) until $\Delta\phi$ is driven to some preset small value. In general, this iteration process is quadratically convergent and does not require many iterations. In many cases, just one pass through Eq. (3) is sufficient to reach good convergence.

Steps 1 and 2 are schematically illustrated in Fig. 1.

Treatment of $(\partial/\partial)\tau(\rho/J)$ in Eq. (1)

$$\frac{\partial}{\partial\tau}\left(\frac{\rho}{J}\right) = \frac{(a_1 - \theta b_1)\left[\left(\frac{\rho}{J}\right)^{n+1} - \left(\frac{\rho}{J}\right)^{n}\right] - \theta b_1\left[\left(\frac{\rho}{J}\right)^{n} - \left(\frac{\rho}{J}\right)^{n-1}\right]}{a_1\Delta\tau_1 - \theta b_1(\Delta\tau_1 + \Delta\tau_2)} \tag{4}$$

where

$$a_1 = (\Delta\tau_1 + \Delta\tau_2)^2, \qquad b_1 = \Delta\tau_1^2,$$

$\theta = 0$ for first-order time accuracy

$\theta = 1$ for second-order accuracy

$$\Delta\tau_1 = \tau^{n+1} - \tau^n, \qquad \Delta\tau_2 = \tau^n - \tau^{n-1}$$

The unknown quantity in Eq. (4) is ρ^{n+1}. Following Eq. (3), this is written as

$$\rho = \rho(\phi_*) + \left(\frac{\partial\rho}{\partial\phi}\right)_{\phi=\phi_*} \Delta\phi \tag{5}$$

where $\Delta\phi = \phi - \phi_*$ and

$$\left(\frac{\partial\rho}{\partial\phi}\right)_{\phi=\phi_*} = \left[-\frac{\rho}{a^2}\left\{\frac{1}{\Delta\tau_1} + U\frac{\partial}{\partial\zeta} + V\frac{\partial}{\partial\eta}\right\}\right]_{\phi=\phi_*} \tag{6}$$

is a differential operator. The density quantities ρ^n and ρ^{n-1} appearing in Eq. (4) are not linearized because they are known. Since ρ^{n+1} is iterated to convergence using Eq. (5), conservation is maintained when $\Delta\phi \to 0$.

Treatment of $\partial/\partial\zeta[\rho(U/J)]$

Following the Newton procedure of Eq. (3),

$$\frac{\partial}{\partial\zeta}\left(\rho\frac{U}{J}\right) = \frac{\partial}{\partial\zeta}\left(f + \frac{\partial f}{\partial\phi}\Delta\phi\right), \quad f = \left(\rho\frac{U}{J}\right)_{\phi=\phi_*}, \quad \Delta\phi = \phi - \phi_* \tag{7}$$

$$\frac{\partial f}{\partial\phi} = \frac{1}{J}\left\{\rho\frac{\partial U}{\partial\phi} + U\frac{\partial\rho}{\partial\phi}\right\} \tag{8}$$

where $(\partial\rho/\partial\phi)$ is given by Eq. (6) and

$$\frac{\partial U}{\partial\phi} = a_{11}\frac{\partial}{\partial\zeta} + a_{12}\frac{\partial}{\partial\eta}$$

For mixed flow calculations where elliptic and hyperbolic regions coexist, inclusion of $(\partial\rho/\partial\phi)$ in Eq. (8) leads to a pentadiagonal matrix due to the term

$$\frac{\partial}{\partial\zeta}\left\{\frac{\rho}{J}\left(a_{11} - \frac{U^2}{a^2}\right)\frac{\partial}{\partial\zeta}\Delta\phi\right\}$$

present in Eq. (8). When $[a_{11} - (U^2/a^2)]$ is negative, this requires upwinding, causing the pentadiagonal feature. To preserve a tridiagonal form for easy and efficient matrix inversion, the term $U(\partial\rho/\partial\phi)$ appearing in Eq. (8) is neglected. Since $\Delta\phi \to 0$ at convergence of Eq. (3), this will not cause any problems.

Equation (7) is written as

$$\begin{aligned}\frac{\partial\left(\rho\frac{U}{J}\right)}{\partial\zeta} &= \left(\tilde{\rho}\frac{U}{J}\right)_{j,k+\frac{1}{2}}^{n+1} - \left(\tilde{\rho}\frac{U}{J}\right)_{j,k-\frac{1}{2}}^{n+1} \\ &= \left[\frac{\tilde{\rho}}{J}\left(\zeta t + a_{11}\{\phi_* + \Delta\phi\}_\zeta + a_{12}\{\phi_* + \Delta\phi\}_\eta\right)\right]_{j,k+\frac{1}{2}} \\ &\quad - \left[\frac{\tilde{\rho}}{J}\left(\zeta t + a_{11}\{\phi_* + \Delta\phi\}_\zeta + a_{12}\{\phi_* + \Delta\phi\}_\eta\right)\right]_{j,k-\frac{1}{2}}\end{aligned} \tag{9}$$

In Eq. (9), the density $\tilde{\rho}$ is given by $\tilde{\rho}(\phi_*)$. The tilde over ρ denotes that the density has been modified to produce the necessary artificial viscosity. The modified density is obtained from a flux biasing concept to be described later in this paper.

Treatment of $\partial/\partial\eta[\rho(V/J)]$

Similarly to Eq. (9), this can be written as

$$\frac{\partial}{\partial\eta}\left(\rho\frac{V}{J}\right) = \left(\tilde{\rho}\frac{V}{J}\right)_{j+\frac{1}{2},k} - \left(\tilde{\rho}\frac{V}{J}\right)_{j-\frac{1}{2},k} \tag{10}$$

where $V = \eta_t + a_{21}(\phi_* + \Delta\phi)_\zeta + a_{22}(\phi_* + \Delta\phi)_\eta$.

Combining Eqs. (4), (9), and (10) results in an implicit treatment of Eq. (1), with $\Delta\phi = \phi - \phi_*$ as the only unknown to be solved for, using the Newton iteration procedure of Eq. (3). To initiate this iterative process, an initial guess for ϕ at $(n+1)$, close to the correct value, is required. This initial guess is provided by solving the time linearized form of Eq. (1) as described now.

Initial Guess

To solve Eq. (1) in a time linearized fashion, the density ρ^{n+1} appearing in Eq. (4) is written as

$$\rho^{n+1} = \rho^n + \left(\frac{\partial\rho}{\partial t}\right)^n \Delta t \tag{11}$$

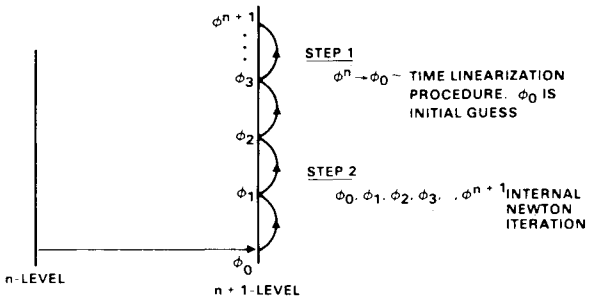

Fig. 1 Update of ϕ based on Newton iteration.

$$\rho^{n+1} = \rho^n + \left(\frac{\partial \rho}{\partial t}\right)^n \Delta\phi \tag{12}$$

where $\Delta\phi = (\phi^{n+1} - \phi^n)$ and

$$\left(\frac{\partial \rho}{\partial \phi}\right)^n = \left[-\frac{\rho}{a^2}\left\{\frac{\partial}{\partial \tau} + U\frac{\partial}{\partial \xi} + V\frac{\partial}{\partial \eta}\right\}\right]^n \tag{13}$$

is a differential operator. In Eq. (12), the density is linearized about a known neighborhood state at the nth level, whereas in Eq. (5) the density is linearized about a known neighborhood state at the $(n+1)$ level. Note the subtle difference in the time terms of Eqs. (6) and (13).

The spatial derivative terms are written as

$$\frac{\partial[\rho/(U/J)]}{\partial \xi} = \frac{\partial}{\partial \xi}\left\{\tilde{\rho}^n \frac{U^{n+1}}{J}\right\}$$

$$\frac{\partial[\rho/(V/J)]}{\partial \eta} = \frac{\partial}{\partial \eta}\left\{\tilde{\rho}^n \frac{V^{n+1}}{J}\right\} \tag{14}$$

where $\tilde{\rho}^n$ is the biased, time linearized density evaluated at the nth plane.

Substituting Eq. (12) into Eq. (4) and combining that with Eq. (14) results in an implicit model for the unknown, $\Delta\phi = \phi^{n+1} - \phi^n$, appearing in Eq. (12). Once this $\Delta\phi$ is solved for, $\phi^{n+1} = \phi^n + \Delta\phi$ provides the initial guess, ϕ_*, needed for the Newton iteration, Eq. (3).

For genuine unsteady problems, at each time plane $n+1$, the Newton iteration is carried out until the residual of the unsteady equation (1) is driven to small values of the order of 10^{-6}. After the initial guess is obtained, two Newton iterations, at the utmost, are generally required to achieve this level of convergence. There are two reasons for this: 1) the initial guess is good, and 2) the Newton iterative process is quadratically convergent. For problems in which the steady state exists and is of interest (steady transonic flow computation), the Newton iteration process is shut off since there is no requirement to satisfy Eq. (1) at every time plane exactly.

Biasing Procedure

The spatial derivative terms given by Eqs. (9), (10), and (14) are central-differenced expressions about the node point (j, k) and are symmetric operators. For shocked flows and for treatment of hyperbolic regions, these operators are desymmetrized by introducing the biased value of density in the upwind direction. This creates the necessary artificial viscosity to form shocks and exclude the expansion shock. The biased value of density $\tilde{\rho}$ can be obtained in several ways, some of which are presented here.

Density Biasing[2] (in the ξ Direction)

$$\tilde{\rho}_{k+\frac{1}{2}} = \rho_{k+\frac{1}{2}} \mp \nu \Delta\xi \left(\frac{\overleftrightarrow{\partial \rho}}{\partial \xi}\right)_{k+\frac{1}{2}}, \quad \nu = \max\left(0, 1 - \frac{1}{M^2}\right)_{k+\frac{1}{2}} \tag{15}$$

where M is the local Mach number. For $U > 0$, the minus sign and backward differencing ($\leftarrow$) are used in Eq. (15), while for $U < 0$, the plus sign and ($\rightarrow$) operator are used.

Directional Flux Biasing

$$\tilde{\rho} = \frac{1}{q}\left\{\rho q \mp \Delta\xi \frac{\partial}{\partial \xi}(\rho q)^-\right\} \tag{16}$$

Streamwise Flux Biasing

$$\tilde{\rho} = \frac{1}{q}\left\{\rho q \mp \Delta S \frac{\partial}{\partial S}(\rho q)^-\right\} \tag{17}$$

where S is the local streamwise direction. Equation (17) can be rearranged as

$$\tilde{\rho} = \frac{1}{q}\left[\rho q \mp \left\{\frac{U}{Q}\Delta\xi \frac{\partial}{\partial \xi} + \frac{V}{Q}\Delta\eta \frac{\partial}{\partial \eta}\right\}(\rho q)^-\right] \tag{18}$$

where $Q = \sqrt{U^2 + V^2}$.

In Eqs. (16) and (18), the term $(\rho q)^-$ is defined to be

$$(\rho q)^- = \rho q - \rho^* q^* \qquad \text{if } q > q^*$$
$$= 0 \qquad \text{if } q \le q^* \tag{19}$$

The quantities $\rho^* q^*$, ρ^*, and q^* represent sonic values of the flux, density, and total velocity, respectively. These sonic conditions are given by (using the density and speed of sound relationships)

$$(q^*)^2 = \frac{1 + [(\gamma-1)/2] M_\infty^2 (1 - 2\phi_\tau - 2\xi_t \phi_\xi - 2\eta_t \phi_\eta)}{(\gamma + 1/2) M_\infty^2}$$

$$\rho^* = (q^* M_\infty)^{2/(\gamma-1)} \tag{20}$$

Note that for steady flows, the sonic conditions ρ^* and q^* are only a function of the freestream Mach number and, for a given flow, they are constants. For unsteady flows, ρ^* and q^* need to be computed everywhere due to the presence of ϕ_τ and other unsteady terms in Eq. (20).

The density biasing based on flux, Eq. (18), is more accurate than the one presented in Eq. (15), since it is based on sonic reference conditions. To illustrate the flux biasing procedure for various situations, Eq. (16) is considered.

1) Subsonic flow [$q < q^*$ at $(j, k+\frac{1}{2})$ and $(j, k-\frac{1}{2})$] for $U > 0$, the modified density in Eq. (16) becomes

$$\tilde{\rho}_{j,k+\frac{1}{2}} = \frac{1}{q_{j,k+\frac{1}{2}}}\left\{(\rho q)_{j,k+\frac{1}{2}} - \left[(\rho q)^-_{j,k+\frac{1}{2}} - (\rho q)^-_{j,k-\frac{1}{2}}\right]\right\}$$
$$= \rho_{j,k+\frac{1}{2}} \tag{21}$$

since $(\rho q)^-$ at $(j, k+\frac{1}{2})$ and $(j, k-\frac{1}{2})$ is zero, according to Eq. (19).

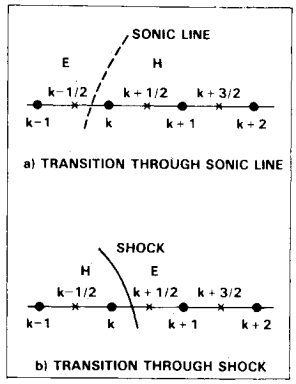

Fig. 2 Notation for flux biasing.

2) Supersonic flow [$q > q^*$ at $(j, k+\frac{1}{2})$ and $(j, k-\frac{1}{2})$] for $U > 0$,

$$\tilde{\rho}_{j,k+\frac{1}{2}} = \frac{1}{q_{j,k+\frac{1}{2}}}\left\{(\rho q)_{j,k+\frac{1}{2}} - \left[(\rho q - \rho^* q^*)_{j,k+\frac{1}{2}} - (\rho q - \rho^* q^*)_{j,k-\frac{1}{2}}\right]\right\}$$
$$= \frac{(\rho q)_{j,k-\frac{1}{2}}}{q_{j,k+\frac{1}{2}}} + \frac{1}{q_{j,k+\frac{1}{2}}} \times \left[\left\{(\rho^* q^*)_{j,k+\frac{1}{2}} - (\rho^* q^*)_{j,k-\frac{1}{2}}\right\}\right] \tag{22}$$

For steady supersonic flows where $(\rho^* q^*)$ is a constant everywhere, Eq. (22) reduces to

$$\tilde{\rho}_{j,k+\frac{1}{2}} = \rho_{j,k-\frac{1}{2}}\left\{\frac{q_{j,k-\frac{1}{2}}}{q_{j,k+\frac{1}{2}}}\right\} \tag{23}$$

3) Transition through sonic line ($q > q^*$ at $k+\frac{1}{2}$ and $q < q^*$ at $k-\frac{1}{2}$. Refer to Fig. 2a.) For $U > 0$,

$$\tilde{\rho}_{j,k+\frac{1}{2}} = \frac{1}{q_{j,k+\frac{1}{2}}}\left\{(\rho q)_{j,k+\frac{1}{2}} - \left[(\rho q - \rho^* q^*)_{j,k+\frac{1}{2}} - (\rho q)^-_{j,k-\frac{1}{2}}\right]\right\} = \frac{\rho^* q^*}{q_{j,k+\frac{1}{2}}} \tag{24}$$

4) Transition through shock ($q > q^*$ at $k-\frac{1}{2}$ and $q < q^*$ at $k+\frac{1}{2}$. Refer to Fig. 2b.) For $U > 0$,

$$\tilde{\rho}_{j,k+\frac{1}{2}} = \frac{1}{q_{j,k+\frac{1}{2}}}\left\{(\rho q)_{j,k+\frac{1}{2}} - \left[(\rho q)^-_{j,k+\frac{1}{2}} - (\rho q - \rho^* q^*)_{j,k-\frac{1}{2}}\right]\right\}$$
$$= \rho_{j,k+\frac{1}{2}} + \frac{1}{q_{j,k+\frac{1}{2}}}\{\rho q - \rho^* q^*\}_{j,k-\frac{1}{2}} \tag{25}$$

For steady flows where $\rho^* q^*$ is a constant, it can be shown that at a pure supersonic point (case 2 above), the flux biasing procedure, Eq. (16), and the usual density biasing technique of Ref. 2, Eq. (15), are identical.

$$\frac{\partial \rho}{\partial q} = -\frac{\rho}{a^2} q \tag{26}$$

$$\frac{\partial \rho}{\partial \xi} = \frac{\partial \rho}{\partial q}\frac{\partial q}{\partial \xi} = -\frac{\rho}{a^2} q q_\xi \tag{27}$$

$$\frac{\partial}{\partial \xi}(\rho q)^- = \frac{\partial}{\partial \xi}(\rho q - \rho^* q^*)$$
$$= \frac{\partial}{\partial \xi}(\rho q) \quad \text{(for steady flows only)}$$
$$= \rho_\xi q + \rho q_\xi \tag{28}$$

Using Eq. (28)

$$\frac{\partial}{\partial \xi}(\rho q)^- = \rho_\xi q\left\{1 - \frac{a^2}{q^2}\right\} = \rho_\xi q\left\{1 - \frac{1}{M^2}\right\} \tag{29}$$

Using Eq. (29), for a pure supersonic point, Eq. (16) becomes, for $U > 0$,

$$\tilde{\rho}_{j,k+\frac{1}{2}} = \frac{1}{q_{j,k+\frac{1}{2}}}\left\{\rho q - \Delta\xi \rho_\xi q\left(1 - \frac{1}{M^2}\right)\right\}_{j,k+\frac{1}{2}} \tag{30}$$

Using $\nu = [1 - (1/M^2)]$, Eq. (30) can be written as

$$\tilde{\rho}_{j,k+\frac{1}{2}} = \rho_{j,k+\frac{1}{2}} - \nu(\rho_{j,k+\frac{1}{2}} - \rho_{j,k-\frac{1}{2}})$$
$$= (1-\nu)\rho_{j,k+\frac{1}{2}} + \nu\rho_{j,k-\frac{1}{2}} \tag{31}$$

Equation (31) is the usual density biasing technique of Holst.[2] However, while transitioning through a sonic line (case 3) or through a shock (case 4), the flux biasing procedure of Eq. (16) accurately monitors the sonic conditions ρ^* and q^*, as given by Eqs. (24) and (25).

The advantages of flux biasing over the density biasing[2] scheme are:

1) It provides a monotone profile through the shock wave (for details, see Refs. 12 and 13).

2) It allows for larger Courant numbers to be taken during the calculation (by not producing undesired pressure overshoots at shocks, which could cause instability during transient calculations).

3) It provides a two-point transition through a shock wave.

The theoretical reason for the validity of properties 1-3, as described in Refs. 13 and 14, is the fact that this flux biasing algorithm satisfies an "entropy" inequality. Consequently, expansion shocks are automatically dissipated—no artificial viscosity involving user-specified constants is needed for this purpose.

The particular flux biasing algorithm described here is based on a simplified solution to a Riemann problem, where a sharp distinction is made between rarefaction waves and expansion shocks. Certain other algorithms based on different approximate (or exact) Riemann solvers are also admissible,[13] but the one used here has the desirable properties of:

1) Smoothness of fluxes—linearization is easy and Newton's method applies directly.

2) An appealing physical interpretation.[14] The method of characteristics is used, even through shocks and the resulting multivalued solution is averaged.

3) Sharp shocks (property 4, transition through shock).

Schemes based on similar principles have already replaced the Murman scheme in transonic small-disturbance codes.[13,14]

Unsteady Wake Treatment

Figure 3 shows the schematic of a wake cut behind the trailing edge of an airfoil. This wake cut has to be properly modeled in the unsteady formulation. An expression for the jump in ϕ across the wake cut can be derived by requiring that the pressure be continuous across the cut. In the full potential framework, this results in the continuity of density. Equating the density $\rho_u = \rho_\ell$ at any point along the wake (Fig. 3), one can write the linearized vorticity (Γ) convection equa-

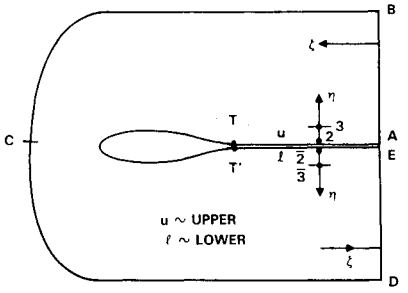

Fig. 3 Wake and outer boundary treatment.

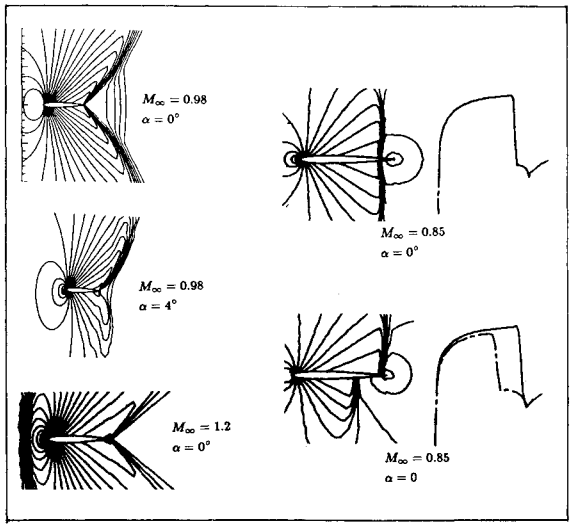

Fig. 4 Steady-state results using the unsteady code.

tion

$$\Gamma_t + U^n \Gamma_\zeta^{n+1} = 0 \tag{32}$$

where U^n is the average of upper and lower cut value at the previous time level. Equation (32) is integrated from the trailing edge to the downstream boundary (along TE in Fig. 3) to obtain the Γ distribution along the wake cut. To maintain stability, the ζ derivatives in Eq. (32) are upwind-differenced. For a steady flow, Eq. (32) will result in a constant value for Γ along the wake given by $\Gamma = \phi_T - \phi_{T'}$ in Fig. 3. Equation (1) is solved only on the upper cut grid points to obtain ϕ_{upper} distribution. Based on the Γ distribution from Eq. (32), the lower cut ϕ values are set ($\phi_\ell = \phi_u - \Gamma$). The jumps in higher derivatives of ϕ such as $|\phi_{\eta\eta}|$, are neglected in the formulation.

Far-Field Boundary Condition

Along the outer boundary ABCDE in Fig. 3, appropriate Riemann invariants are prescribed. The concept can be explained by considering the Cartesian form of the full potential equation cast in terms of the Riemann invariants.

$$\frac{\partial}{\partial t}\left(u + \frac{2}{\gamma-1}a\right) + (u+a)\frac{\partial}{\partial x}\left(u + \frac{2}{\gamma-1}a\right) = 0$$

$$\frac{\partial}{\partial t}\left(u - \frac{2}{\gamma-1}a\right) + (u-a)\frac{\partial}{\partial x}\left(u - \frac{2}{\gamma-a}a\right) = 0 \tag{33}$$

Equation (33) implies that along the $(u+a)$ positive characteristics, the quantity $\{u + [2/(\gamma-1)]a\}$ is invariant and, along the $(u-a)$ negative characteristics, the quantity $\{u - [2/(\gamma-1)]a\}$ is invariant, known as the Riemann invariants. Usually, along the outer boundary, the Riemann invariant that corresponds to the positive characteristics with respect to the inward normal can be prescribed as a boundary condition. For an arbitrary coordinate system (τ, ζ, η), such as the one in Fig. 3, the following boundary conditions are appropriate.

$$\frac{U}{\sqrt{a_{11}}} + \frac{2}{\gamma-1}a = \text{const along AB}$$

$$-\frac{U}{\sqrt{a_{11}}} + \frac{2}{\gamma-1}a = \text{const along ED}$$

$$-\frac{V}{\sqrt{a_{22}}} + \frac{2}{\gamma-1}a = \text{const along BCD} \tag{34}$$

Equation (34) is nonlinear in nature. Hence, to implement the Riemann invariant boundary condition, a linearization technique similar to Eq. (3) is employed. For example, equating the right-hand side of Eq. (34) to the freestream value, along BCD one can write

$$-\left[\left(a_{12}\frac{\partial}{\partial\zeta} + a_{22}\frac{\partial}{\partial\eta}\right)\Delta\phi\right]\Big/\left(\sqrt{a_{22}}\right)$$

$$-\frac{1}{a}\left(\frac{1}{\Delta\tau} + U\frac{\partial}{\partial\zeta} + V\frac{\partial}{\partial\eta}\right)\Delta\phi$$

$$= \left(-\frac{V}{\sqrt{a_{22}}} + \frac{2}{\gamma-1}a\right)_{\text{freestream}}$$

$$-\left(-\frac{VF}{\sqrt{a_{22}}} + \frac{2}{\gamma-1}a\right) \tag{35}$$

where $\Delta\phi = \phi - \phi_*$. All the coefficients in Eq. (35) are evaluated using $\phi = \phi_*$. The finite-differenced form of Eq. (35) will provide an estimate for $(\Delta\phi)$ along the outer boundary.

Approximate Factorization Scheme

Equation (1), modeled in terms of the unknown, $\Delta\phi = \phi - \phi_*$, can be written as

$$G(\Delta\phi) + R(\phi_*, \phi^n, \phi^{n-1}, \cdots) = 0 \tag{36}$$

Equation (36) can be solved in several ways. One way is to apply a relaxation technique that uses either a point iteration or line relaxation.[15] In this paper, the method of approximate factorization[4-6] is chosen over the relaxation concept. In the approximate factorization procedure, the $G(\Delta\phi)$ function in Eq. (36) is written as

$$L_\zeta L_\eta \Delta\phi = R \tag{37}$$

where

$$L_\zeta = \left[1 + \Delta\tau_1 U\frac{\partial}{\partial\zeta} + \frac{\alpha}{\beta}\frac{\partial}{\partial\zeta}\frac{\tilde{\rho}^*}{J}a_{11}\frac{\partial}{\partial\zeta}\right]$$

$$L_\eta = \left[1 + \Delta\tau_1 V\frac{\partial}{\partial\eta} + \frac{\alpha}{\beta}\frac{\partial}{\partial\eta}\frac{\tilde{\rho}^*}{J}a_{22}\frac{\partial}{\partial\eta}\right]$$

$$\beta = -\left(\frac{\rho}{J^{n+1}(a\Delta\tau_1)^2}\right)_{j,k}$$

$$\alpha = (1-\theta) + \theta\left[\{a_1 - b_1(\Delta\tau_1 + \Delta\tau_2)/\Delta\tau_1\}/\{a_1 - b_1\}\right]$$

Equation (37) is solved at the $(n+1)$ plane in two steps.

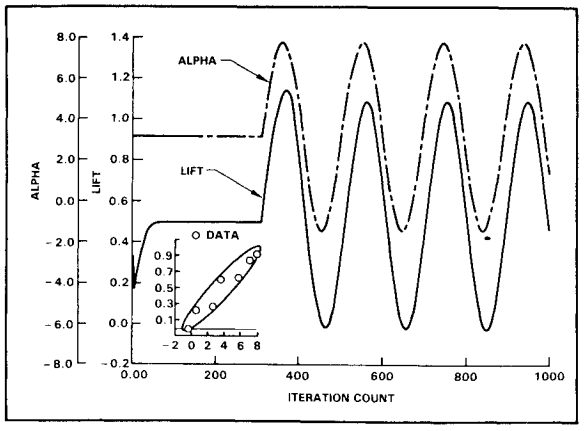

Fig. 5 Variation of unsteady lift with α for NACA-0012 at $k = 0.081$, $M_\infty = 0.6$, $\alpha_m = 3.16$ deg, $\alpha_0 = 4.59$ deg.

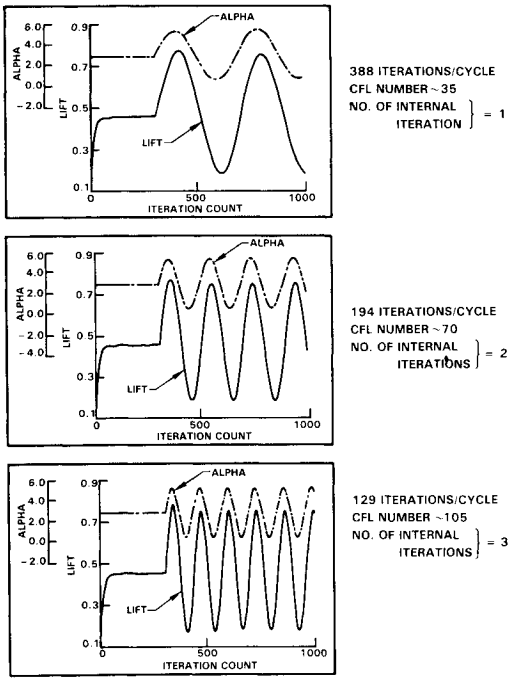

Fig. 6 Test of robustness of the present unsteady implicit scheme. NACA-0012 airfoil at $M_\infty = 0.6$, $k = 0.081$, $\alpha_m = 2.89$ deg, $\alpha_0 = 2.41$ deg.

Step 1:

$$L_\zeta \overline{\Delta\phi} = R$$

Step 2:

$$L_\eta \Delta\phi = \overline{\Delta\phi}$$

$$\phi_{j,k}^{n+1} = \phi_* + \Delta\phi_{j,k}$$

Both L_ζ and L_η result in tridiagonal matrices.

Body Boundary Condition

For inviscid flows, the surface flow tangency condition dictates that the contravariant velocity V be zero at the body. Implementation of the condition $V = 0$ in the L_η operator is a crucial step in achieving a true implicit scheme. Usually, the boundary condition $V = 0$ is set only in the right-hand-side term R, and a careless or no-boundary-condition treatment is imposed in the left-hand-side L_η operator[2]. In the present method, the condition $V = 0$ is imposed on both sides of Eq. (37). Let $j = J$ denote the body point. Then,

$$V = \left(\eta_t + a_{12}\phi_\zeta + a_{22}\phi_\eta\right)_{J,k} = 0 \tag{38}$$

or

$$\left(\phi_\eta\right)_{J,k} = -\left(\frac{a_{12}}{a_{22}}\phi_\zeta\right)_{J,k} - \left(\frac{\eta_t}{a_{22}}\right)_{J,k} \tag{39}$$

Using Eqs. (38) and (39) and the relationship

$$\left(\rho\frac{V}{J}\right)_{J-\frac{1}{2}} = -\left(\rho\frac{V}{J}\right)_{J+\frac{1}{2}} \tag{40}$$

the L_ζ and the L_η operators in Eq. (37) can be modified to the form, for a body point J,

$$\tilde{L}_\zeta \tilde{L}_\eta \Delta\phi = \tilde{R} \tag{41}$$

where

$$\tilde{L}_\zeta = \left[1 + \Delta\tau_1 U \frac{\partial}{\partial\zeta} + \frac{\alpha}{\beta}\frac{\partial}{\partial\zeta}\frac{\tilde{\rho}}{J}\left(a_{11} - \frac{a_{12}^2}{a_{22}}\right)\frac{\partial}{\partial\zeta}\right]$$

$$\tilde{L}_\eta = \left[1 + \frac{2}{\Delta\eta}\frac{\alpha}{\beta}\left(\frac{\tilde{\rho}}{J}a_{22}\frac{\partial}{\partial\zeta}\right)_{J+\frac{1}{2}}\right]$$

In Eq. (41), the boundary condition is split between the two operators $\tilde{L}_\zeta$ and $\tilde{L}_\eta$. Even for nonorthogonal mesh at the body ($a_{12} \neq 0$), the boundary condition is set implicitly. This allows for large time steps, or Courant numbers, to be taken during the calculation.

While solving for a wake point, Eq. (1) and Eq. (32) are solved simultaneously (implicitly) through proper modification to the L_η operator in Eq. (37).

Extension to Three Dimensions

The two-dimensional procedure described so far is easily extended to three dimensions by introducing a triple approximate factorization scheme. This is represented as

$$L_\xi L_\zeta L_\eta \Delta\phi = R \tag{42}$$

Reference 16 describes the three-dimensional implementation.

III. Results

The computer program based on the implicit method of this paper is written for the CRAY-XMP computer. The program is vectorized, including the tridiagonal solvers of the approximate factorization scheme, and the flux biasing switches. Usually, calculations are performed on a 181×30 c-grid setup. For steady-state calculations, the method takes approximately 200 iterations (with no internal Newton iterations) to drive the residual values to 10^{-5} or less, and this takes 3.3 s/100 iterations on the CRAY-XMP. For unsteady calculations, the code initially sets up the steady solutions about the mean airfoil position and then performs the unsteady calculation. To maintain time accuracy, internal Newton iterations are performed to drive the residual of the unsteady equation to less than 10^{-5}. Usually, two internal iterations are sufficient. However, when large $\Delta\tau$ values that correspond to CFL numbers of over 100 are used, more internal iterations might be required. For unsteady calculations with two internal iterations after the initial guess from the time linearized solution (see Fig. 1), the code requires 9.0 s/100 iterations.

Now, some results are presented.

Figure 4 shows the fishtail shock pattern for the steady NACA-0012 airfoil at Mach numbers 0.98 and 1.2. The present method computes difficult cases like these in 200 iterations

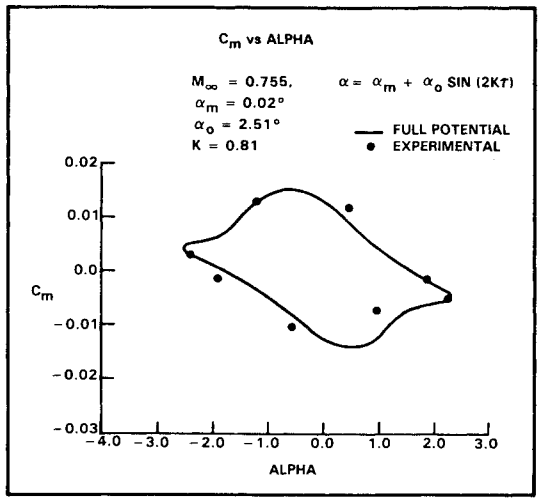

Fig. 7a Comparison of unsteady pitching moment coefficient.

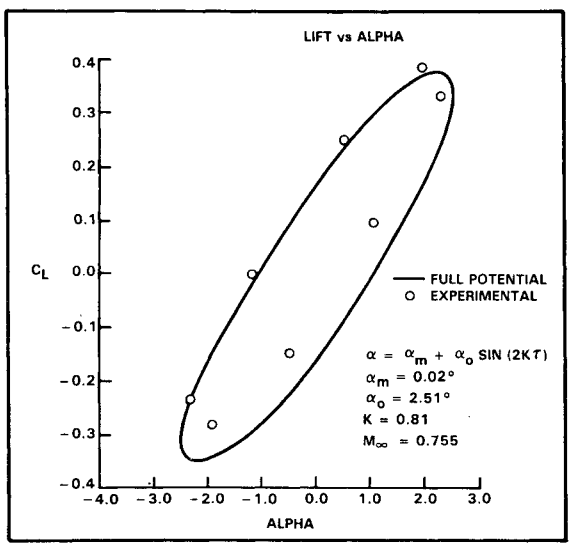

Fig. 7b Comparison of unsteady lift coefficient.

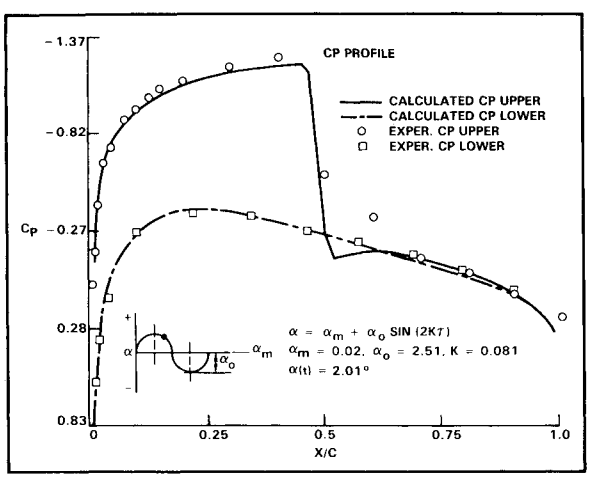

Fig. 7c Comparison of unsteady pressures for NACA-0012, $\alpha(t) = 2.01$ during downswing.

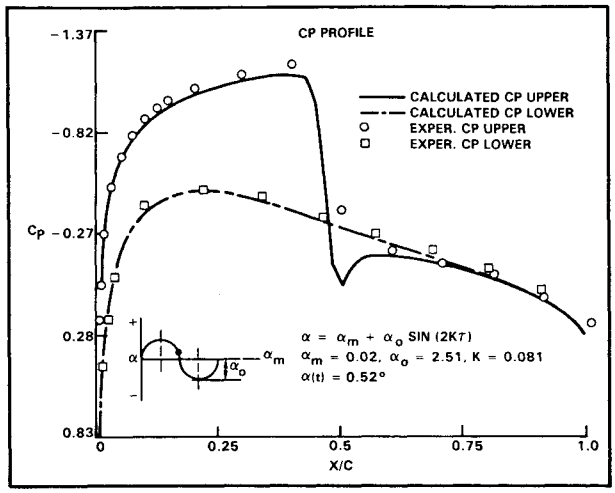

Fig. 7d Comparison of unsteady pressures for NACA-0012, $\alpha(t) = 0.52$ during downswing.

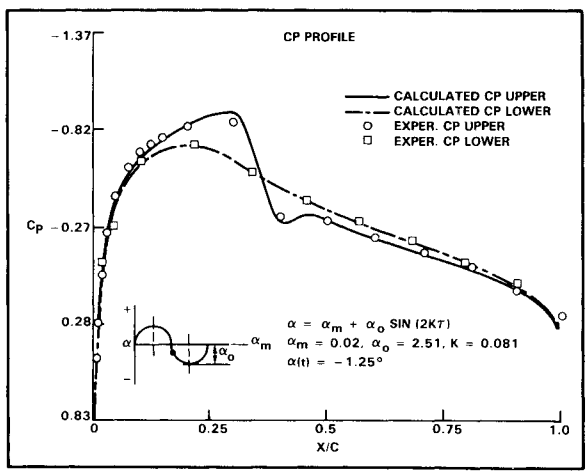

Fig. 7e Comparison of unsteady pressures for NACA-0012, $\alpha(t) = -1.25$ during downswing.

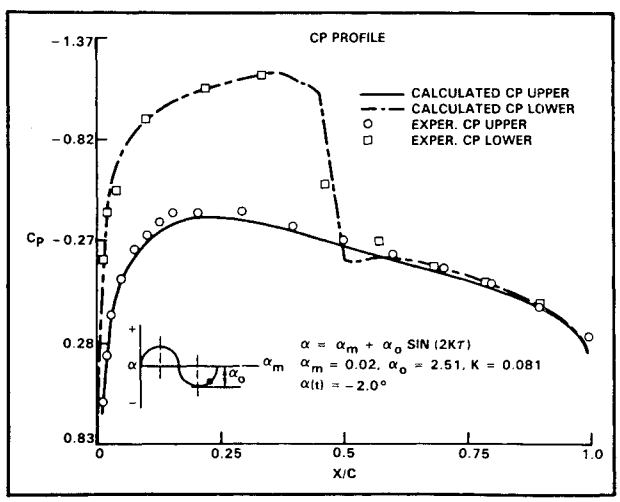

Fig. 7f Comparison of unsteady pressures for NACA-0012, $\alpha(t) = -2.0$ during upswing.

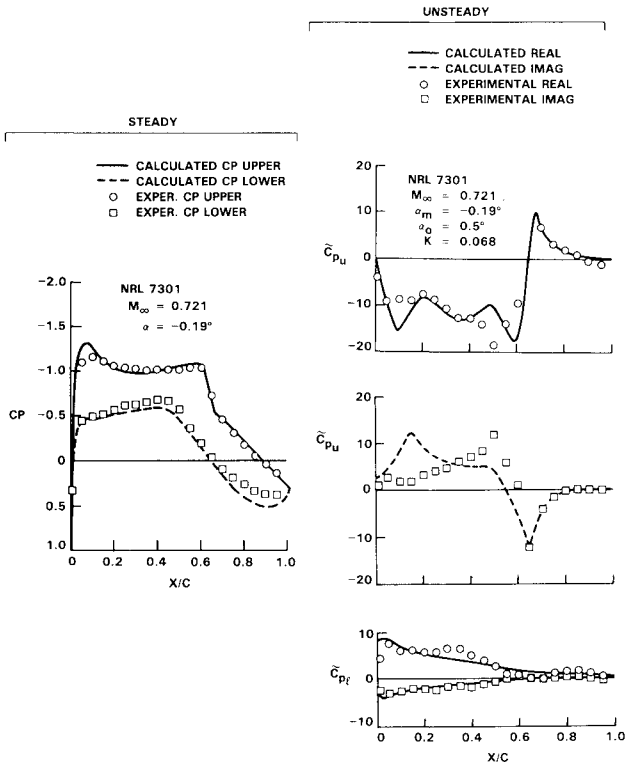

Fig. 8 Steady and unsteady results for the NLR-7301 airfoil.

without requiring any code adjustments. Use of the flux biasing concept accurately treats any complex shock problem and provides the correct amount of artificial viscosity for stability and accuracy. Also shown in Fig. 4 are results for $M_\infty = 0.85$, indicating the presence of nonuniqueness,[17] even for the unsteady full potential equation.

Figure 5 shows an unsteady calculation for NACA-0012 at a reduced frequency, $k = (w/2)(U_\infty/c)$, of 0.081. The airfoil is pitching about the quarter-chord and the angle of attack is given by

$$\alpha = \alpha_m + \alpha_0 \sin \omega t$$

where α_m is the mean angle and α_0 is the amplitude.

Unsteady calculations are started after 300 iterations of steady-state computation about the mean position. For a low reduced frequency of 0.081, the airfoil sets into an unsteady periodic motion very quickly (within a cycle of transient motion). The unsteady result of Fig. 5 was performed using 190 iterations/cycle at an average CFL number of 65. The unsteady lift coefficients compare well with data.[18] The outer boundary of the computational domain was set at 20 chord lengths away.

To test the robustness and accuracy of the present method, unsteady calculations were performed, for a given case, using different $\Delta\tau$ values. Figure 6 shows the results of such a study. For NACA-0012, $M_\infty = 0.6$, $k = 0.081$, $\alpha_m = 2.89$, $\alpha_0 = 2.41$ deg, three different $\Delta\tau$ values were chosen ($\Delta\tau = 0.1, 0.2, 0.3$) that correspond to average CFL numbers of 35, 70, and 105, respectively. For $\Delta\tau = 0.1$, one cycle of calculation required 388 iterations and, for $\Delta\tau = 0.3$, the same required 130 iterations. The code performed very well and produced stable results for all these three cases, producing the same C_ℓ vs α loop within plottable accuracy.

Figures 7a-7f show unsteady results for a strongly shocked NACA-0012 airfoil at $M_\infty = 0.755$, $\alpha_M = 0.02$, $\alpha_0 = 2.59$, and $\kappa = 0.081$. The unsteady variation in pitching moment coefficient (about a quarter-chord), C_M, is shown in Fig. 7a, along with a comparison with experimental data.[18] Figure 7b shows similar results for the lift coefficient variation. Figures 7c-7f show unsteady pressures on the surface at various orientations of the pitching airfoil. In all these results, the comparison with experimental data[18] is excellent. Similar results obtained using the transonic small-disturbance theory are shown in Ref. 19.

Figure 8 shows steady and unsteady results for the NLR-7301 airfoil oscillating in pitch about 40% chord. The experimental data are from Ref. 19.

IV. Conclusions

The paper presents a fast, time-accurate, unsteady full potential scheme based on the Newton iteration concept applied to approximate factorization. The method has incorporated the following key features.

1) Conservative treatment of the unsteady full potential equation, 2) time linearization procedures for computing the initial guess for the internal Newton iteration, 3) flux biasing techniques based on sonic reference conditions for production of artificial viscosity to capture shocks and treat the hyperbolic regions, 4) implicit boundary condition treatment based on splitting concepts consistent with approximate factorization, 5) treatment of unsteady wake by properly accounting for jumps in ϕ, and 6) outer boundary conditions based on the Riemann invariants.

Currently, work is progressing in the following areas: 1) inclusion of a structural model for aeroelastic and flutter calculations, 2) interacting boundary-layer method for treating viscous effects, 3) unified scheme development for across-the-Mach-number capability,[12] 4) "entropy correction" to extend the range of validity of the unsteady full potential equation, and 5) wing-body treatment.

V. Acknowledgments

The authors express thanks to Drs. Chakravarthy and Szema of Rockwell for many valuable discussions. This work was partially funded by NASA Langley Research Center under Contract NAS1-15820.

References

[1]Jameson, A., "Transonic Potential Flow Calculations using Conservation Form," *Proceedings of the AIAA 2nd Computational Fluid Dynamic Conference*, 1975, pp. 148-155.

[2]Holst, T.L., "Fast, Conservative Algorithm for Solving the Transonic Full Potential Equation," *AIAA Journal*, Vol. 18, Dec. 1980, pp. 1431-1439.

[3]Siclari, M.J., "Computation of Nonlinear Supersonic Potential Flow over Three-Dimensional Surfaces," AIAA Paper 82-0167, Jan. 1982.

[4]Shankar, V., "A Conservative Full Potential, Implicit, Marching Scheme for Supersonic Flows," *AIAA Journal*, Vol. 20, Nov. 1982, pp. 1508-1514.

[5]Shankar, V. and Osher, S., "An Efficient Full Potential Implicit Method Based on Characteristics for Analysis of Supersonic Flows," AIAA Paper 82-0974, June 1982; *AIAA Journal*, Vol. 21, Sept. 1983, p. 1262.

[6]Shankar, V., Szema, K.-Y., and Osher, S., "Treatment of Supersonic Flows with Embedded Subsonic Regions," *AIAA Journal*, Vol. 23, Jan. 1985, pp. 41-48.

[7]Chipman, R. and Jameson, A., "An Alternating Direction Implicit Algorithm for Unsteady Potential Flow," AIAA Paper 81-0329, Jan. 1981.

[8]Goorjian, P.M., "Computations of Unsteady Transonic Flow Governed by the Conservative Full Potential Equation using an Alternating Direction Implicit Algorithm," NASA CR-152274, June 1979.

[9]Sankar, N.L. and Tassa, Y., "An Algorithm for Unsteady Transonic Potential Flow Past Airfoils," 7th International Conference on Numerical Methods in Fluid Dynamics, June 1980.

[10]Steger, J. and Caradonna, F., "A Conservative Implicit Finite Difference Algorithm for the Unsteady Transonic Full Potential Equation," AIAA Paper 80-1368, July 1980.

[11]Malone, J.B. and Sankar, N.L., "Numerical Simulation of 2-D Unsteady Transonic Flows using the Full Potential Equation," AIAA Paper 83-0233, 1983.

[12]Shankar, V., "A Unified Full Potential Scheme for Subsonic, Transonic, and Supersonic Flows," AIAA Paper 85-1643, 1985.

[13]Osher, S., Hafez, M., and Whitlow, W. Jr., "Entropy Condition Satisfying Approximations for the Full Potential Equation of Transonic Flow," *Mathematics of Computation*, Vol. 44, No. 169, Jan. 1985, pp. 1-29.

[14]Hafez, M., Whitlow, W. Jr., and Osher, S., "Improved Finite Difference Schemes for Transonic Flow Calculations," AIAA Paper 84-0092, Jan. 1984.

[15]Chakravarthy, Sukumar, "Implicit Upwind Schemes without Approximate Factorization," AIAA Paper 84-0165, Jan. 1984.

[16]Shankar, V. and Hiroshi, I., "Treatment of Steady and Unsteady Three-Dimensional Flows Using a Time-Accurate Full Potential Scheme," AIAA Paper 85-4060, Oct. 1985.

[17]Steinhoff, J. and Jameson, A., "Multiple Solutions of the Transonic Potential Flow Equation," AIAA Paper 81-1019, 1981.

[18]"Compendium of Unsteady Aerodynamic Measurements," AGARD R-702, Aug. 1982.

[19]Edwards, J.W., Bland, S.R., and Seidel, D.A., "Experience with Transonic Unsteady Aerodynamic Calculation," NASA TM 86278, Aug. 1984.